AGU PUBLICATIONS

Geophysical Research Letters

RESEARCH LETTER
10.1002/2017GL074862

**Key Points:**
- More than 2 years of electric drift measurements by the Van Allen Probes are compared with theoretical models below 2 Earth radii
- Assuming a rigidly rotating ionosphere is enough to predict the average spatial variations of the radial component of the electric drift
- Accounting for the thermospheric winds in the model improves the predictions of the average azimuthal component of the electric drift

**Supporting Information:**
- Supporting Information S1

**Correspondence to:**
S. Lejosne,
solene@ssl.berkeley.edu

**Citation:**
Lejosne, S., S. Maus, and F. S. Mozer (2017), Model-observation comparison for the geographic variability of the plasma electric drift in the Earth's innermost magnetosphere, *Geophys. Res. Lett.*, *44*, 7634–7642, doi:10.1002/2017GL074862.

Received 8 JUL 2017
Accepted 27 JUL 2017
Accepted article online 31 JUL 2017
Published online 13 AUG 2017



# Model-observation comparison for the geographic variability of the plasma electric drift in the Earth's innermost magnetosphere

**Solène Lejosne[1], Stefan Maus[2], and F. S. Mozer[1]**

[1]Space Sciences Laboratory, University of California, Berkeley, California, USA, [2]Cooperative Institute for Research in Environmental Sciences (CIRES), University of Colorado Boulder, Boulder, Colorado, USA

**Abstract** Plasmaspheric rotation is known to lag behind Earth rotation. The causes for this corotation lag are not yet fully understood. We have used more than 2 years of Van Allen Probe observations to compare the electric drift measured below $L \sim 2$ with the predictions of a general model. In the first step, a rigid corotation of the ionosphere with the solid Earth was assumed in the model. The results of the model-observation comparison are twofold: (1) radially, the model explains the average observed geographic variability of the electric drift; (2) azimuthally, the model fails to explain the full amplitude of the observed corotation lag. In the second step, ionospheric corotation was modulated in the model by thermospheric winds, as given by the latest version of the horizontal wind model. Accounting for the thermospheric corotation lag at ionospheric *E* region altitudes results in significantly better agreement between the model and the observations.

## 1. Introduction

Even in the innermost magnetosphere below 3 Earth radii ($R_E$), the electric drift $\mathbf{E}\times\mathbf{B}/B^2$ does not set the plasma into rigid corotation, contrary to what is assumed in simple models. Observations of particle dynamics suggested that the electric drift varied with magnetic local time in both radial [*Selesnick et al.*, 2016] and azimuthal [*Gallagher et al.*, 2005; *Galvan et al.*, 2010] directions. In the azimuthal direction, there were also indications that the plasma rotational rate was typically 5 to 10% slower than the planetary rotational rate [*Sandel et al.*, 2003; *Burch et al.*, 2004; *Galvan et al.*, 2010]. Recent analysis of electric and magnetic field measurements demonstrated that the instruments on board Van Allen Probes had the accuracy required to deliver consistent evaluations of the electric drift in a frame of reference fixed to the stars, even below 3 Earth radii [*Lejosne and Mozer*, 2016a, 2016b]. The first results were welcomed as much-needed ground truth in a region of space historically deprived from in situ electric field measurements due to the technical challenges involved [*Mozer*, 2016]. The existence of a corotation lag and the dependence of the electric drift on magnetic local time were confirmed. The study also indicated the existence of a secondary dependence of the electric drift on geographic longitude [*Lejosne and Mozer*, 2016b]. While the magnetic local time dependence of the electric drift was shown to be consistent with that of the ionospheric wind dynamo below $L \sim 2$ and with that of a solar wind-driven convection electric field above $L \sim 2$, the existence of a corotation lag and the electric drift variability with geographic longitude were both left unexplained. The objective of this study is to test if these unsolved features can be clarified by accurately accounting for the Earth's corotation electric field [*Maus*, 2017].

The Geocentric Solar Ecliptic (GSE) frame, which does not corotate with the Earth, can be used as an (almost) inertial frame of reference. The electric field $\mathbf{E}$ in the inertial frame is the sum of the change of the magnetic vector potential ($\mathbf{E_A} = -\partial\mathbf{A}/\partial t$) and the electric field of induced charges ($\mathbf{E_c}$).

$$\mathbf{E} = \mathbf{E_C} + \mathbf{E_A}. \tag{1}$$

Up to the top of the ionospheric *E* region, at about 130 km altitude above the Earth surface, the ionosphere is dragged along by collisions with the corotating neutral thermosphere. For perfect corotation, the electric field $\mathbf{E}'$ in the frame of the corotating ionosphere is then

$$\mathbf{E}' = \mathbf{E_C} + \mathbf{E_A} + (\boldsymbol{\Omega_E}\times\mathbf{r})\times\mathbf{B}, \tag{2}$$

where $\mathbf{B}$ is the magnetic field vector at the location $\mathbf{r}$, and $\boldsymbol{\Omega_E}$ is the Earth's rotation vector. Since the electric

field in a reference frame comoving with the conductor has to be zero ($\mathbf{E}' = 0$), the electric field of the induced charges ($\mathbf{E_C}$) must cancel out the primary electric field, leading to

$$\mathbf{E_C} = -\mathbf{E_A} - (\mathbf{\Omega_E} \times \mathbf{r}) \times \mathbf{B}. \quad (3)$$

This brings the total electric field at the top of the *E* region in the inertial frame to

$$\mathbf{E} = -\mathbf{E_A} - (\mathbf{\Omega_E} \times \mathbf{r}) \times \mathbf{B} + \mathbf{E_A} = -(\mathbf{\Omega_E} \times \mathbf{r}) \times \mathbf{B}. \quad (4)$$

Since the induced charges can move freely along the geomagnetic field lines out into the plasmasphere, equation (3) becomes applicable everywhere within the region of closed field lines, setting into motion the entire plasmasphere [*Maus*, 2017]. As for the electric drift $\mathbf{E} \times \mathbf{B}/B^2$ , it corresponds to the projection of the corotational motion $\mathbf{\Omega_E} \times \mathbf{r}$ in a direction perpendicular to the magnetic field:

$$\frac{\mathbf{E} \times \mathbf{B}}{\mathbf{B}^2} = (\mathbf{\Omega_E} \times \mathbf{r}) - ((\mathbf{\Omega_E} \times \mathbf{r}) \cdot \mathbf{B}) \frac{\boldsymbol{B}}{B^2}. \quad (5)$$

In practice, because the magnetic field is nonaxially symmetric [e.g., *Maus et al*., 2010], the predicted electric drift equation (5) depends on geographic longitude, and the resulting variations could be enough to account for the geographic variability observed by the Van Allen Probes. In some longitudinal sectors, the corotational motion $\mathbf{\Omega_E} \times \mathbf{r}$ has a nonzero component along the magnetic field direction ($(\mathbf{\Omega_E} \times \mathbf{r}) \cdot \mathbf{B} \neq 0$). Therefore, the amplitude of the electric drift is smaller than corotation when averaged over all longitudinal sectors: $\|\mathbf{E} \times \mathbf{B}/B^2\| < \|\mathbf{\Omega_E} \times \mathbf{r}\|$. As a result, this model could possibly explain the observed corotational lag.

One underlying assumption of this model is that the thermospheric neutrals are themselves in rigid corotation with the Earth. Yet deviations exist. High-altitude ionospheric winds could even cause variations in the azimuthal distribution of radiation belt intensity up to $L \sim 3$ [*Lejosne and Roederer*, 2016]. Nonetheless, we first assumed that these time-dependent deviations from rigid corotation canceled when averaged over a day.

## 2. Processing the Van Allen Probe Measurements Below $L = 3$

We examined spin-period-averaged measurements (~12 s) of the electric and magnetic fields from both Van Allen Probes A and B between October 2012 and December 2014. The electric field measurements are from the Electric Field and Waves experiment (EFW) [*Wygant et al*., 2013], and the magnetic field measurements are from the Electric and Magnetic Field Instrument Suite and Integrated Science (EMFISIS) [*Kletzing et al*., 2013]. The Van Allen Probes have an apogee at about 5.8 Earth radii and a perigee at about 600 km. The locations of the apogee and perigee slowly drift in time so that it takes a bit less than 2 years to scan all local time sectors. The spacecraft have an orbital period of about 9 h and an inclination of ~10°. Because of the ~10° offset between magnetic and geographic equators, the electric drifts were measured at solar magnetic latitudes between −20° and +20°. A data-preprocessing technique was applied to derive the most accurate evaluations of the electric drift $\mathbf{E} \times \mathbf{B}/B^2$ from Van Allen Probe raw measurements:

1. First, we corrected a slight misalignment in the magnetometer axes for both spacecraft [*Lejosne and Mozer*, 2016a, 2016b].
2. Second, we replaced the data from the less reliable short-axis electric field antenna by the assumption that the parallel electric field is zero, because of the plasma's high conductivity parallel to magnetic field lines.
3. Finally, the shorting factor was set to 1. The shorting factor is a scaling factor that multiples electric field measurements to correct for the fact that electric potential contours around the spacecraft are distorted by the presence of the spacecraft and long booms. Because below $L \sim 3$ the plasma density is high, the Debye length is short, and this shorting factor effect is unimportant.

Then, we converted each resulting three-dimensional measurement of the electric drift $\mathbf{E} \times \mathbf{B}/B^2$ to a two-dimensional vector, in a local orthonormal frame of reference ($\mathbf{e_\rho}$, $\mathbf{e_b}$, and $\mathbf{e_\varphi}$) set by the *measured* magnetic field direction:

$$\mathbf{e_b} = \frac{-\mathbf{B}}{\|\mathbf{B}\|} \tag{6}$$

$$\mathbf{e_\varphi} = \frac{\mathbf{B}\times\mathbf{r}}{\|\mathbf{B}\times\mathbf{r}\|}, \tag{7}$$

and

$$\mathbf{e_\rho} = \frac{\mathbf{e_\varphi}\times\mathbf{B}}{\|\mathbf{B}\|}, \tag{8}$$

where **B** is the measured magnetic field vector at the location **r**.

By definition, the electric drift has a zero component along $\mathbf{e_b}$. In the two other directions, we defined the following: the *radial* component of the measured electric drift $V_\rho$:

$$V_\rho = \left(\frac{\mathbf{E}\times\mathbf{B}}{\mathbf{B}^2}\right)\cdot\mathbf{e_\rho} \tag{9}$$

and the *azimuthal* component of the measured electric drift $V_\varphi$:

$$V_\varphi = \left(\frac{\mathbf{E}\times\mathbf{B}}{\mathbf{B}^2}\right)\cdot\mathbf{e_\varphi}. \tag{10}$$

At the same time, using information on spacecraft location and measured magnetic field direction, we also computed the *predicted* two-dimensional electric drift, following equation (5). We defined the following: the radial component of the predicted electric drift $U_\rho$:

$$U_\rho = (\mathbf{\Omega_E}\times\mathbf{r})\cdot\mathbf{e_\rho} \tag{11}$$

and the azimuthal component of the predicted electric drift $U_\varphi$:

$$U_\varphi = (\mathbf{\Omega_E}\times\mathbf{r})\cdot\mathbf{e_\varphi}. \tag{12}$$

The objective was to compare the database of *measured* electric drifts ($V_\rho$ and $V_\varphi$), with the database of *predicted* electric drifts ($U_\rho$ and $U_\varphi$).

## 3. Results: Model-Observation Comparison for the Geographic Variability of the Electric Drift in the Earth's Innermost Magnetosphere

Since the geomagnetic field is larger than all changing external contributions from magnetospheric current systems close to Earth, the predicted electric drift ($U_\rho$, $U_\varphi$) depends above all on geographic location. On the other hand, the measured electric drift ($V_\rho$, $V_\varphi$) varies also with magnetic local time and magnetic activity. We chose to disregard the variability of the electric drift with magnetic activity for this study because more than 80% of the measurements were sampled during geomagnetic quiet times ($Kp \leq 2$, $|Dst| \leq 20$ nT). Even so, the number of dimensions involved remained high. In an attempt to simplify the approach, we first present a model-observation comparison in a spatially limited sector that was arbitrarily chosen.

### 3.1. Model-Observation Comparison at $L$ = 1.4 (±0.1) for a Geographic Longitude Between 210 and 230°East

In this case, we also evaluated the predicted electric drifts numerically, based on the International Geomagnetic Reference Field. We used the Fortran IRBEM library [*Boscher et al.*, 2012] to trace magnetic field lines at $L$ = 1.4 with an apex between 210 and 230° in geographic longitude. As different magnetic latitudes (MLAT) were scanned along the field lines, we computed the components of the electric drift following equations (11) and (12). The results are represented in green in Figure 1. The *predicted* electric drift deduced from spacecraft location and magnetic field measurements is presented in red. The *measured* electric drift is plotted in black.

The predicted electric drift components based on spacecraft location and magnetic field measurements (in red) agree well with the numerical reference values (in green), especially in the radial direction (Figure 1a). In the azimuthal direction, the experimental predictions (in red) are more scattered than the numerical predictions (in green). The primary reason for that difference is that the width of the window in $L$ has been set to ±0.1 around $L$ = 1.4. This 0.2 width in $L$ leads to variations of the azimuthal component of the

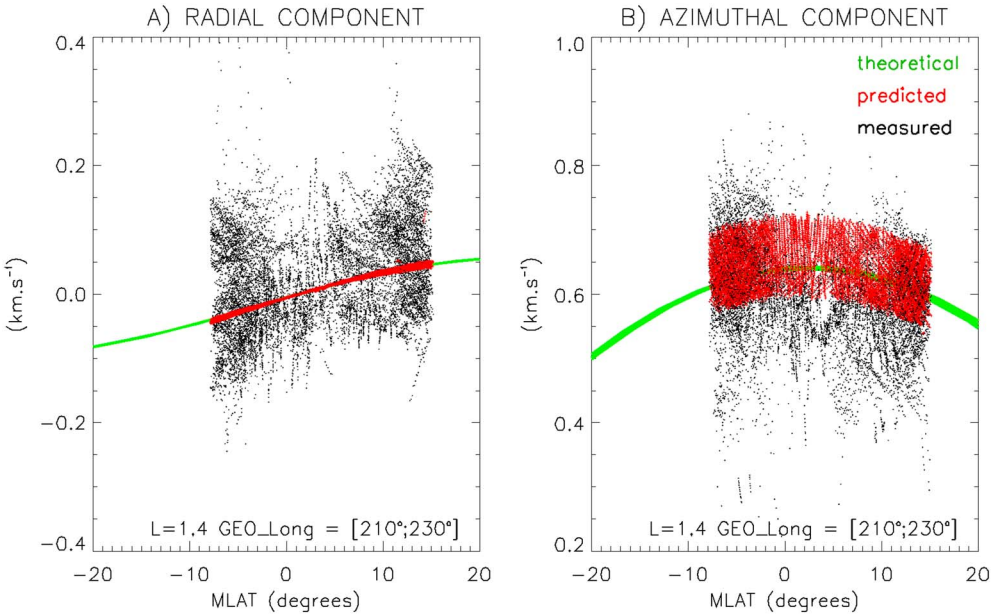


**Figure 1.** Comparison between numerical evaluations of the predicted electric drift (in green), predicted electric drift components based on spacecraft location and magnetic field measurements (in red), and measured electric drifts (in black), in both (a) radial and azimuthal directions, as a function of spacecraft magnetic latitude (MLAT).

electric drift of the order of 0.2 $\Omega_E R_E \sim 0.1$ km $s^{-1}$, observable Figure 1b. To mitigate such variability, we compare in the following predicted and observed *corotation factors* rather than predicted and observed *azimuthal velocities*, dividing the latest by $\|\mathbf{\Omega_E} \times \mathbf{r}\|$.

The good agreement between the numerical evaluations (in green) and the experimental predictions (in red) indicates that there is no significant difference between the modeled and measured directions of the magnetic field in that sector.

As for the experimental electric drift (in black), we note that the measured components are scattered around the predicted values, especially in the radial direction. In the azimuthal direction, the measured component is on average smaller than the predicted ones. In the following, we show that these features are ubiquitous.

### 3.2. Overall Model-Observation Comparison

To sort the databases, we defined 5 bins in *L* shell, ranging from 1.2 to 2, with a step of 0.2 and a width of ±0.1; 24 bins in geographic longitude (GEO), ranging from 0° to 345°, with a step of 15° and a width of ±7.5°, and 8 bins in magnetic local time (MLT), from 0 h to 21 h, with a step of 3 h and a width of ±1.5 h. The sizes of the bins were chosen to be big enough to contain a statistically significant number of samples and small enough to maintain a good spatial resolution for the results. Each data subset contained a least 60 points (1200 points on average). For both databases of predicted and measured electric drifts, for every component, and in every bin, we defined a *typical* value as the median of the corresponding data subset. In the azimuthal direction, rather than storing the corresponding component of the electric drift, we stored the *corotation factor*, defined as the ratio between the azimuthal component of the electric drift and $\|\mathbf{\Omega_E} \times \mathbf{r}\|$. Another possible choice for the definition of the corotation factor is discussed and presented in the supporting information. In a first approximation, one can consider that a corotation factor of 1 indicates a perfect plasmaspheric corotation, a corotation factor below 1 represents subcorotation, and a corotation factor above 1 indicates supercorotation.

To mitigate the MLT dependence of the measured electric drifts, we averaged the typical values over the 8 MLT bins. That way, we canceled variations of the electric drift that have a 24 h periodicity (due to the ionospheric wind dynamo for example). The results are presented in Figure 2.

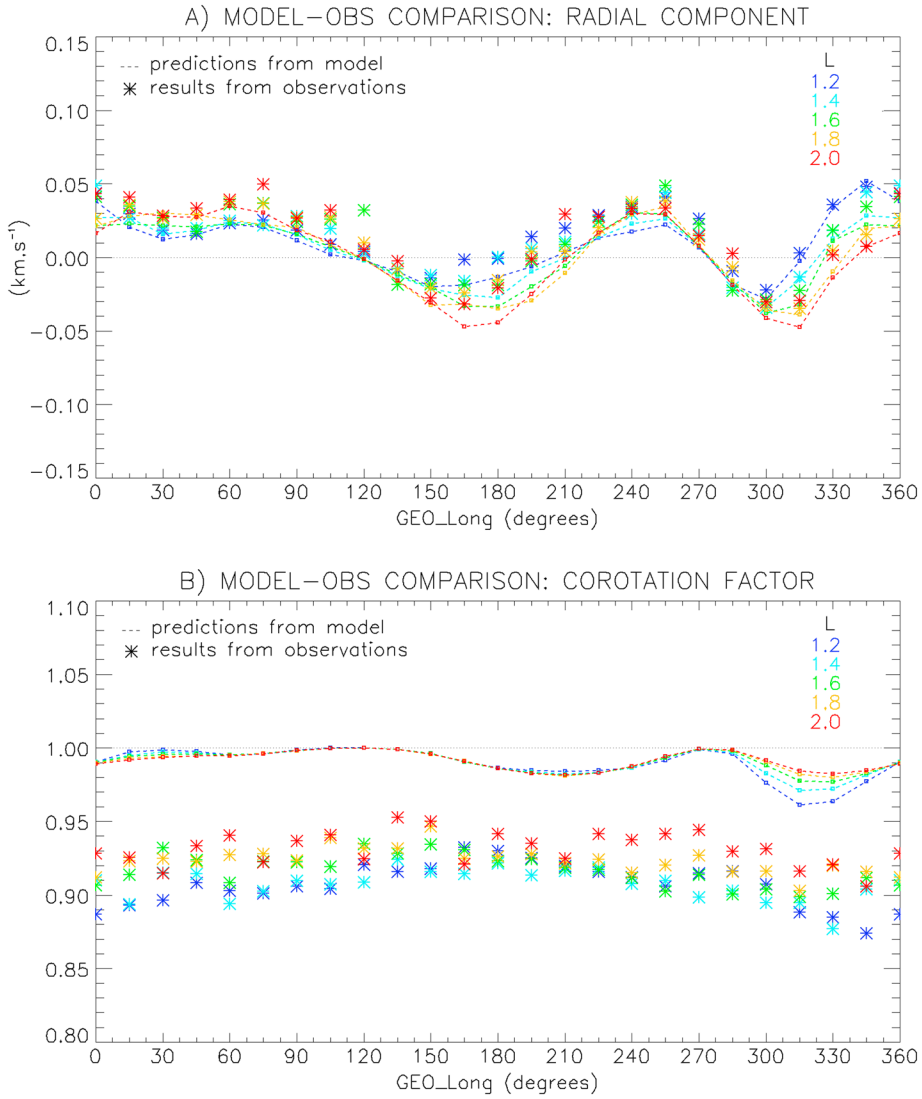


**Figure 2.** Model-observation comparison of the MLT-averaged typical values for the (a) radial component of the electric drift and for the (b) corotation factor. The values predicted from spacecraft location and magnetic field measurements are represented by the dashed line, while the values derived to the Van Allen Probe electric and magnetic field measurements are represented by the asterisk symbols. The *L* shell parameter is color coded.

Figure 2 shows that both predicted and measured radial electric drifts (Figure 2a) and corotation factors (Figure 2b) do not primarily depend on *L*. It shows also that the observed variations of the electric drift with geographic longitude are well reproduced by the model, in particular in the radial direction. However, in the azimuthal direction, although the model predicts some corotational lag [*Maus*, 2017], it underestimates the amplitude of the measured one. The difference between the predicted corotation factors and the observed ones is of the order of 0.08, i.e., about 0.08 $\Omega_E r$, a value which is comprised between ~40 m $s^{-1}$ and ~80 m $s^{-1}$ below $L = 2$. This is more than any difference observed between the measured and predicted typical values of the radial component.

For the predicted electric drift, it is possible to understand the observed variations with geographic longitude in light of the different panels displayed in Figure 3. It shows that the radial component presents a strong dependence on both geographic longitude and latitude (Figure 3a), unlike the corotation factor (Figure 3b). Because different longitudinal sectors were sampled at different magnetic latitudes (Figure 3c), the observed variability of the electric drift with geographic longitude (Figure 2) is a combination of both magnetic latitude and geographic longitude dependence.

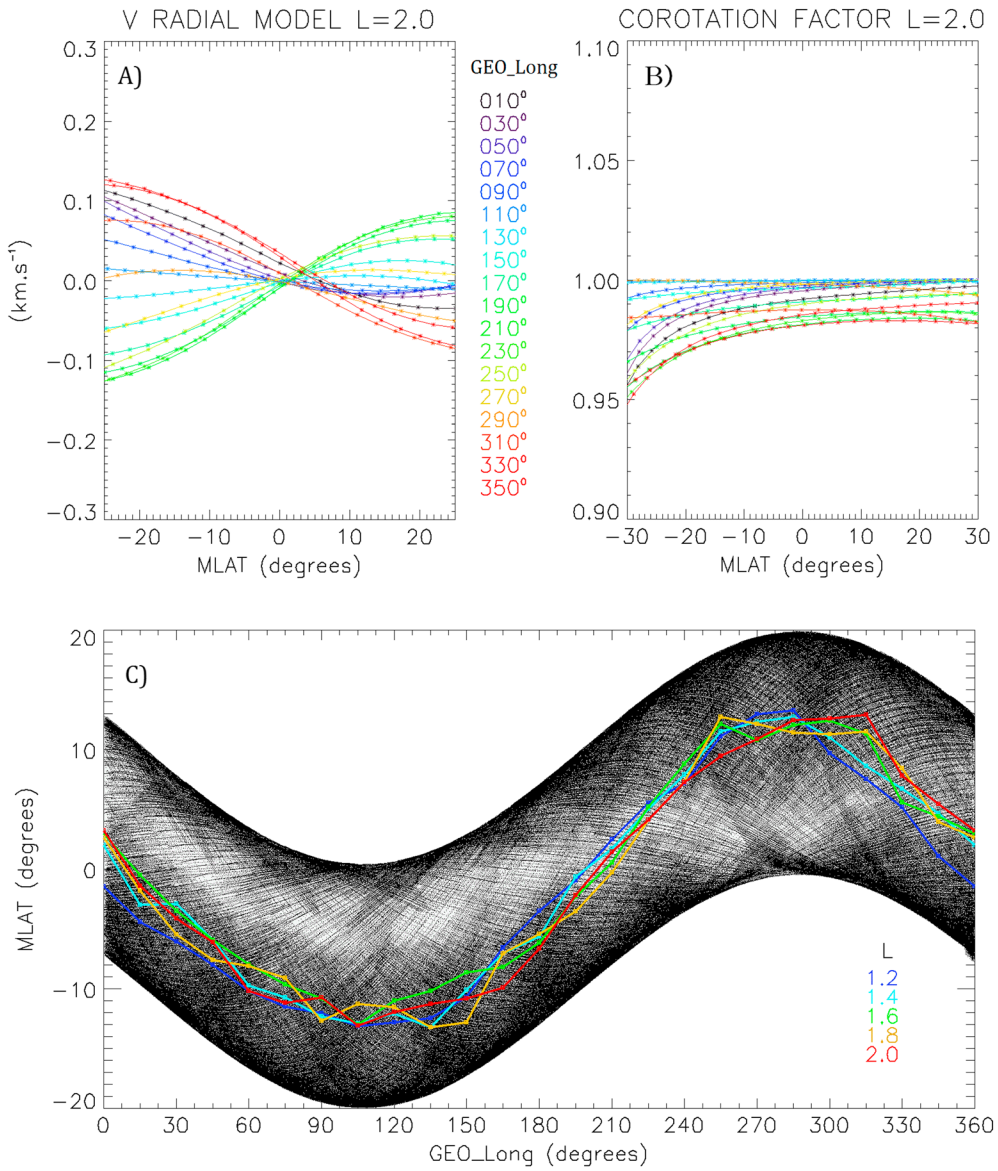


**Figure 3.** (a) The numerical evaluations of the radial component of the electric drift $(\mathbf{\Omega}_\mathbf{E} \times \mathbf{r}) \cdot \mathbf{e}_\rho$ at $L = 2$, as a function of the solar magnetic latitude (MLAT) and for different geographic longitudes (GEO_long). (b) The numerical evaluations of the corotation factor $(\mathbf{\Omega}_\mathbf{E} \times \mathbf{r}) \cdot \mathbf{e}_\varphi / \|\mathbf{\Omega}_\mathbf{E} \times \mathbf{r}\|$ at $L = 2$, as a function of the solar magnetic latitude (MLAT) for different geographic longitudes (GEO_long). (c) The locations of Van Allen Probe measurements (black dots), as well as the typical latitudinal sectors sampled as a function of $L$ (color coded). To obtain the typical locations, we applied the same binning-averaging approach to the magnetic latitude database as the one applied to electric drift measurements.

## 4. Discussion

### 4.1. Nonzero-Induced Electric Fields in the Earth's Innermost Magnetosphere Question Standard Technique for Electric Drift Mapping

In previous works [e.g., *Lejosne and Mozer*, 2016a, 2016b], the components of the electric drift ($V_\rho$, $V_\varphi$) at a given magnetic colatitude $\theta$ were considered to be proportional to the components of the electric drift at the minimum-B locus of the same equipotential field line ($V_{0,\rho}$, $V_{0,\varphi}$).

$$V_\rho(\theta) = \frac{V_{0,\rho}}{R(\theta)} \tag{13}$$

and

$$V_\varphi(\theta) = \frac{V_{0,\varphi}}{F(\theta)}, \tag{14}$$

where $R$ and $F$ are positive amplification factors. With a magnetic dipole for example, $R(\theta) = \sqrt{1+3\cos^2\theta}/\sin^3\theta$ and $F(\theta) = \sin^{-3}\theta$ [*Mozer*, 1970]. As a field line is scanned from the magnetic equator toward the ionosphere, each component of the electric drift is expected to decrease while preserving its sign (either positive or negative). The amplification factors $R$ and $F$ can be derived using Faraday loops [*Toivanen et al*., 1998], assuming that the rate of change of magnetic flux across the surface considered is zero (e.g., supporting information in *Lejosne and Mozer* [2016b]). With a nonaxially symmetric magnetic field, the assumption that the rate of change of magnetic flux is zero is valid *only on average* over the rotation of the Earth. Locally, the assumption does not hold true in a frame of reference fixed to the stars. The electric field presented equation (1) has indeed a component induced by the variation of the magnetic field:

$$\nabla\times\mathbf{E} = (\mathbf{\Omega_E}\times\mathbf{r})\cdot\nabla\mathbf{B} = -\frac{\partial\mathbf{B}}{\partial t}. \tag{15}$$

In particular, it is noticeable in Figures 1a, 2a, and 3a that the radial component of the electric drift cancels and changes sign as it is sampled at different magnetic latitudes along the same field line. In previous work, we concluded that the projection of the electric drift to the magnetic equator was typically outward around 240°E [*Lejosne and Mozer*, 2016b, Figure 4c]. In the light of this analysis, this result should be seen as an artifact due to inaccurate mapping along magnetic field lines. The additional conclusion that the Van Allen Probes measurements confirmed the existence of a plasmaspheric wind [*Lemaire and Schunk*, 1992] should be withdrawn accordingly.

### 4.2. On the Origin of the Observed Corotation Lag

The origin of the corotation lag was first discussed by *Burch et al*. [2004] based on IMAGE extreme ultraviolet observations between $L \sim 2$ and $L \sim 4$. The corotation lag was shown to be fully consistent with the subcorotation of the ionosphere measured by DMSP F12, F13, and F15 satellites. No strong local-time dependence was observed. The latter result discarded the potential role a solar wind convection electric field could play. Instead, *Burch et al*. [2004] identified the *ionospheric disturbance dynamo* [*Blanc and Richmond*, 1980] as the cause of the rotation lag. Yet this theory was later questioned by *Galvan et al*. [2010] and *Lejosne and Mozer* [2016a].

In this work, we show that the lag between the predicted and observed corotation factors is present at all geographic longitudes, at all observed magnetic latitudes. Because the variations of the azimuthal component of the electric drift with MLT were found to be consistent with the ionospheric wind dynamo below $L \sim 2$ [*Lejosne and Mozer*, 2016a], it appears that the corotation lag does not even occur in a localized MLT region.

We therefore conclude that the existence of a corotation lag is a persistent feature, observed everywhere below at least $L \sim 2$. As a result, we question the underlying assumption that the thermospheric neutrals are on average in rigid corotation with the Earth. In particular, we use the latest version of the horizontal wind model (HWM14) [*Drob et al*., 2015] to estimate the velocity of the thermospheric neutrals. HWM is an empirical model that provides a global and time-dependent specification of the thermospheric wind patterns from the surface to the exobase (at an altitude of ~450 km) based on more than 50 years of satellite and ground-based data. In place of $\Omega_E$, we correct each data point for the *predicted* electric drift by a small $(\Omega_E + \delta\Omega)/\Omega_E$ factor, where $\delta\Omega$ represents the estimated variation of the angular velocity due to high-altitude winds. Every $\delta\Omega$ is computed at the field line foot points under the following assumptions:

1. We consider that the neutral atmosphere drags along the ions up to an altitude of ~130 km, altitude at which the gyrofrequency exceeds the collision frequency [*Kelley*, 2009, Figure 2.5 p.44]. The ions then rearrange in such a way that there is no net electric field for a charge comoving with the atmosphere. This sets up the potential along the field lines that forces the plasmasphere to corotate. In reality, there is a smooth transition rather than a sharp cutoff at 130 km.
2. Because the HWM14 model shows differences in the wind speed between the southern and northern intersect points, we make the ad hoc first-order assumption that the resulting corotation factor is simply the average of the corotation factors of the two points. This approach also averages out noise in the wind model.

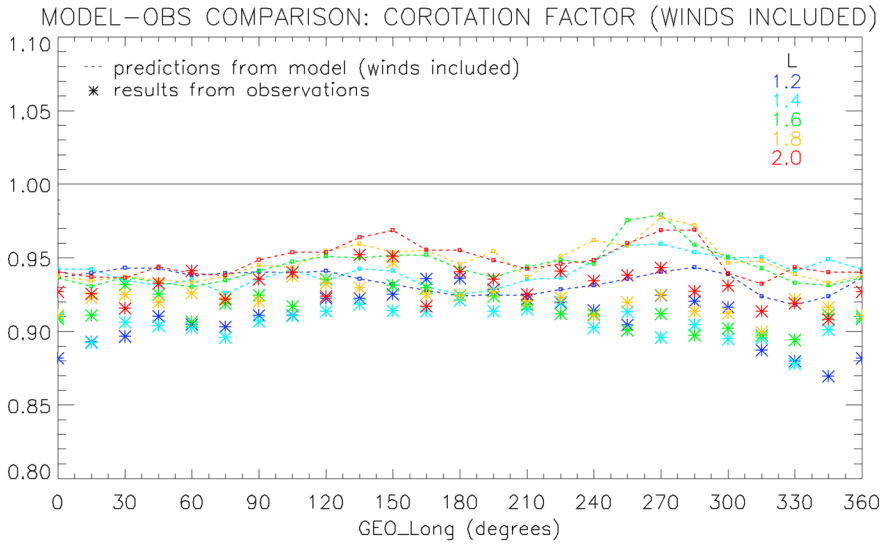


**Figure 4.** Model-observation comparison of the typical values of the corotation factor. The values predicted from spacecraft location and magnetic field measurements taking into account the thermosphere neutral winds are represented by the dashed line, while the values derived from Van Allen Probe electric and magnetic field measurements are represented by the asterisk symbols. The *L* shell parameter is color coded.

We then compute the new set of predicted typical values and we compare with the observed ones. The results are presented in Figure 4. More detailed results, comparing model and observation as a function of magnetic local time, are provided in the supporting information.

The comparison of Figure 4 with Figure 2b shows that the inclusion of high-altitude winds in the electric drift model leads to additional subcorotation in the predicted values. The new predicted values agree better with the observations (with a decrease of about a factor 2 in the differences between predictions and observations). However, the observed corotational lag remains slightly stronger than the predicted one. We nevertheless consider this as a strong indication that the subcorotation of the plasmasphere is related to the subcorotation of the thermospheric neutrals.

Although thermospheric winds vary with location and magnetic local time (supporting information), Figure 4 indicates also that the thermospheric neutrals in HWM14 have an average westward motion (easterly wind) with respect to the Earth at 130 km of altitude. To our best knowledge, such easterly wind is unknown.

Assuming this average westward motion is a real feature of the thermospheric neutrals at 130 km of altitude, this neutral drag should also translate in an overall westward motion of the ionosphere. Therefore, one would expect studies of ion drift ground-based measurements to also report on an overall westward drift of the ionosphere [*Lejosne and Mozer*, 2016a]. Why this is not the case remains currently unexplained. However, to observe this average westward ion drift would require high-accuracy measurements with a 24 h continuous coverage. Therefore, one could speculate that this overall westward drift, of the order of only a few tens of m $s^{-1}$, is too small to be resolved by most instruments.

**Acknowledgments**
The data used in this paper are available at the Van Allen Probe website: http://rbspgway.jhuapl.edu/. The Fortran Library International Radiation Belt Environment Modeling (IRBEM-LIB) was used for the numerical computations of the electric drift prediction. IRBEM-LIB can be downloaded at http://sourceforge.net/projects/irbem/. The authors thank the scientists and engineers associated with the EFW and EMFISIS instruments for providing the high-quality data reported in this paper. The work of S.L. and F.M. was performed under JHU/APL Contract No. 922613 (RBSP-EFW). S.M. was supported by NASA grant NNX13AL20G.

## References

Blanc, M., and A. Richmond (1980), The ionospheric disturbance dynamo, *J. Geophys. Res.*, 297 *85* (A4), 1669–1686, doi: 10.1029/JA085iA04p01669.

Boscher, D., S. Bourdarie, P. O'Brien, and T. Guild (2012), *IRBEM Library*, Version 4.4.0.

Burch, J. L., J. Goldstein, and B. R. Sandel (2004), Cause of plasmasphere corotation lag, *Geophys. Res. Lett.*, *31*, L05802, doi:10.1029/2003GL019164.

Drob, D. P., et al. (2015), An update to the horizontal wind model (HWM): The quiet time thermosphere, *Earth Space Sci.*, *2*, 301–319, doi:10.1002/2014EA000089.

Gallagher, D. L., M. L. Adrian, and M. W. Liemohn (2005), Origin and evolution of deep plasmaspheric notches, *J. Geophys. Res.*, *110*, A09201, doi:10.1029/2004JA010906.

Galvan, D. A., M. B. Moldwin, B. R. Sandel, and G. Crowley (2010), On the causes of plasmaspheric rotation variability: Image EUV observations, *J. Geophys. Res.*, *115*, A01214, doi:10.1029/2009JA014321.

Kelley, M. C. (2009), *The Earth's Ionosphere, Plasma Physics and Electrodynamics*, 2nd ed., Elsevier.

Kletzing, C. A., et al. (2013), The Electric and Magnetic Field Instrument Suite and Integrated Science (EMFISIS) on RBSP, *Space Sci. Rev.*, *179*, 127–181, doi:10.1007/s11214-013-993-3066.

Lejosne, S., and F. S. Mozer (2016a), Van Allen Probe measurements of the electric drift $\mathbf{E} \times \mathbf{B}/B^2$ at Arecibo's $L$ = 1.4 field line coordinate, *Geophys. Res. Lett.*, *43*, 6768–6774, doi:10.1002/2016GL069875.

Lejosne, S., and F. S. Mozer (2016b), Typical values of the electric drift $\mathbf{E} \times \mathbf{B}/B^2$ in the inner radiation belt and slot region as determined from Van Allen Probe measurements, *J. Geophys. Space Physics*, *121*, doi:10.1002/2016JA023613.

Lejosne, S., and J. G. Roederer (2016), The "zebras stripes": An effect of *F* region zonal plasma drifts on the longitudinal distribution of radiation belt particles, *J. Geophys. Res. Space Physics*, *121*, doi:10.1002/2015JA021925.

Lemaire, J. F., and R. W. Schunk (1992), Plasmaspheric wind, *J. Atmos. Terr. Phys.*, *54*, 467–477, doi:10.1016/0021-9169(92)90026-H.

Maus, S. (2017), A corotation electric field model of the Earth derived from Swarm satellite magnetic field measurements, *J. Geophys. Res. Space Physics*, *122*, doi:10.1002/2017JA024221.

Maus, S., C. Manoj, J. Rauberg, I. Michaelis, and H. Lühr (2010), NOAA/NGDC candidate models for the 11th generation international geomagnetic reference field and the concurrent release of the 6th generation Pomme magnetic model, *Earth Planets Space*, *62*(10), 2, doi:10.5047/eps.2010.07.006.

Mozer, F. S. (1970), Electric field mapping in the ionosphere at the equatorial plane, *Planet. Space Sci.*, *18*, 259–263, doi:10.1016/0032-0633(70)90161-3.

Mozer, F. S. (2016), DC and low frequency double probe electric field measurements in space, *J. Geophys. Res. Space Physics*, *121*, doi:10.1002/2016JA022952.

Sandel, B. R., J. Goldstein, D. L. Gallagher, and M. Spasojevic (2003), EUV observations of the structure and dynamics of the plasmasphere, *Space Sci. Rev.*, *109*, 25–46, doi:10.1023/B:SPAC.0000007511.47727.5b.

Selesnick, R. S., Y.-J. Su, and J. B. Blake (2016), Control of the innermost electron radiation belt by large-scale electric fields, *J. Geophys. Res. Space Physics*, *121*, 8417–8427, doi:10.1002/2016JA022973.

Toivanen, P. K., H. E. J. Koskinen, and T. I. Pulkkinen (1998), Mapping between the ionospheric and the tail electric fields in a time-dependent Earth's magnetosphere, *J. Geophys. Res.*, *103*(A5), 9153–9164, doi:10.1029/97JA03028.

Wygant, et al. (2013), The electric field and wave instruments on the Radiation Belt Storm Probes Mission, *Space Sci. Rev.*, *179*, 183–220, doi:10.1007/s11214-013-0013-7.